
This is an electronic reprint of the original article.

This reprint may differ from the original in pagination and typographic detail.

Latypova, Renata; Nyo, Tun Tun; Kauppi, Timo; Pallaspuuro, Sakari; Mehtonen, Saara; Hänninen, Hannu; Kömi, Jukka

Hydrogen-induced stress corrosion cracking studied by the novel tuning-fork test method

Published in:
Materials and Corrosion

DOI:
[10.1002/maco.202011767](https://doi.org/10.1002/maco.202011767)


Published: 01/10/2020

Document Version
Publisher's PDF, also known as Version of record

Published under the following license:
CC BY

Please cite the original version:
Latypova, R., Nyo, T. T., Kauppi, T., Pallaspuuro, S., Mehtonen, S., Hänninen, H., & Kömi, J. (2020). Hydrogen-induced stress corrosion cracking studied by the novel tuning-fork test method. *Materials and Corrosion*, 71(10), 1629-1636. <https://doi.org/10.1002/maco.202011767>

Hydrogen-induced stress corrosion cracking studied by the novel tuning-fork test method

Renata Latypova¹  | Tun Tun Nyo¹ | Timo Kauppi^{1,2} | Sakari Pallaspuro¹ |
Saara Mehtonen³ | Hannu Hänninen⁴ | Jukka Kömi¹

¹Materials and Mechanical Engineering,
Centre for Advanced Steels Research
(CASR), University of Oulu, Oulu, Finland

²Arctic Steel and Mining RDI Group,
Lapland University of Applied Science,
Kemi, Finland

³SSAB, Raahe, Finland

⁴Department of Mechanical Engineering,
Aalto University School of Engineering,
Espoo, Finland

Correspondence

Renata Latypova, Materials and
Mechanical Engineering, Centre for
Advanced Steels Research (CASR),
University of Oulu, P.O. Box 4200,
90014 Oulu, Finland.
Email: renata.latypova@oulu.fi

Abstract

A novel tuning-fork test method was developed to study hydrogen-induced stress corrosion cracking of high-strength steels. Special tuning-fork specimens are designed to enable accurate stress adjustment via constant displacement under cathodic hydrogen charging conditions. In this study, the testing method is further developed, making the potentiostatic hydrogen charging possible through the modifications of the corrosion cell. Different direct-quenched, low- and medium-carbon steel grades, with a hardness range of 300–550 HBW, are investigated with both galvanostatic and potentiostatic hydrogen charging techniques. For each steel grade, the lowest fracture stress and highest no-fracture stress are determined. Both hydrogen charging techniques produce similar results, and it is observed that the fracture stress decreases with the increase in hardness. However, the potentiostatic technique produces larger differences between the lowest fracture stress results, thus having a better resolution.

KEYWORDS

hydrogen charging, hydrogen embrittlement, steel, stress corrosion cracking

1 | INTRODUCTION

Direct-quenched steels with high strength and hardness, as well as sufficient toughness, are widely used in transportation as well as in processing and mining industries, where they are exposed to adhesive and abrasive wear conditions.^[1,2] High-strength steels have many advantages, as they enable lighter structures, which result in cost savings, but they also increase the risk of stress corrosion cracking (SCC), which can lead to a catastrophic failure.^[3] SCC occurs for a susceptible material, which is subjected to a high enough tensile stress in a specific corrosion environment.^[4] For high-strength steels, the predominant SCC mechanism

is hydrogen embrittlement (HE) or hydrogen-induced stress corrosion cracking (HISCC).^[5,6]

There are a number of metallurgical variables that strongly influence the susceptibility to HE, one of which is the strength or the hardness level of the steel.^[7,8] In general, a greater strength level leads to a higher HE susceptibility, and failures caused by HE are often encountered with high-strength steels.^[8,9] For example, in the mining industry, where abrasion-resistant direct-quenched steels are often exploited, the mineral content of the mine water can result in the breakdown of the iron sulphate minerals, which eventually produces sulphuric acid, H₂SO₄. Consequently, the low pH of the mine water

This is an open access article under the terms of the Creative Commons Attribution License, which permits use, distribution and reproduction in any medium, provided the original work is properly cited.

© 2020 The Authors. *Materials and Corrosion* published by Wiley-VCH Verlag GmbH & Co. KGaA

accelerates the breakdown of minerals, and the corrosion reactions with steel produce hydrogen. The formed hydrogen can diffuse into the material and, with a critical concentration, cause HE.^[10]

The occurrence of HE depends on three factors: a source of hydrogen, transportation processes to the location where embrittlement occurs and the embrittlement mechanism itself.^[5] In the case of HISCC, hydrogen originates from the cathodic corrosion reactions, which can occur in almost any acidic environment.^[11] Highly mobile monoatomic or nascent hydrogen can dissolve and rapidly diffuse into the metal through interstitial sites, leading from high-concentration (surface) to low-concentration (interior or opposite surface) regions.^[6,11] Hydrogen diffuses readily to regions under high triaxial tensile stresses as the expanding lattice allows greater mobility, accumulating hydrogen at trapping sites, such as dislocations, grain boundaries and inclusions, and finally leading to crack initiation and propagation.^[12]

To evaluate the susceptibility of high-strength steels to HISCC, different types of hydrogen charging experiments are conducted with various loading methods such as constant displacement, constant strain, constant load and linearly increasing load.^[5] Electrochemical hydrogen charging can be performed under both galvanostatic and potentiostatic conditions. The galvanostatic method applies constant cathodic current (two-electrode set-up) to the test specimen, and it is more commonly used when compared with the potentiostatic technique, which utilises constant cathodic potential (three-electrode set-up).^[13,14] The distinguishing factor between these two techniques is the essential need for a reference electrode during the potentiostatic hydrogen charging, whereas the galvanostatic technique requires only a power source.^[14] The reference electrode does not pass current, but it allows to measure the potential of the working electrode. With galvanostatic set-up, measuring the potential of the working electrode is not possible.^[15] According to the Nernst equation (Equation 1), hydrogen activity in metal a_H depends on the applied potential E

$$E = E_0 + \frac{RT}{F} \ln a_H, \quad (1)$$

where E_0 is the standard electrode potential of metal on the standard electrode series, T is the temperature during hydrogen charging, R is the gas constant and F is Faraday's constant. The benefit of the potentiostatic method is that the applied constant potential will provide the same activity of hydrogen for all the studied steels during the hydrogen charging experiments.^[16–18]

The novel tuning-fork test (TFT) and its test specimen geometry were recently developed for the testing of high-strength steels via a constant displacement under cathodic hydrogen charging conditions.^[19] This practical test method eliminated stress control issues with a novel specimen geometry combined with a simple, yet effective, clamping system operated by hand. The applied stress states were verified with a finite element method (FEM) model. In this sense, the use of traditional specimens, such as C-ring^[20,21] or U-bend^[22,23] specimens, is not ideal, because forming/bending process of high-strength steels can be difficult to perform identically, requiring specialised equipment. TFT is also considerably cheaper to perform, compared with the testing methods that require tensile testing equipment. However, the original TFT set-up was limited only to the galvanostatic hydrogen charging. In this study, the TFT method was developed further to enable the potentiostatic hydrogen charging by the modifications of the corrosion cell.

2 | MATERIALS AND METHODS

2.1 | Specimen geometry and preparation

All experiments were carried out with test specimens manufactured from direct-quenched, hot-rolled steel sheets with nominal hardness levels of 300, 400, 500 and 550 HBW. Table 1 presents the carbon content and mechanical properties of the studied steels as provided by the supplier.

Tuning-fork specimens underwent wire electrical discharge machining after cutting the steel strips into sheets (50 × 150 mm), and machining 0.5 mm from both surfaces to achieve the final 5-mm thickness.^[19] The tuning-fork specimen geometry, with arrows marking the rolling direction of the sheet, is presented in Figure 1.

TABLE 1 Carbon content (in wt%) and mechanical properties of the test materials

Steel grade (HBW)	C	Measured hardness (HBW)	0.2% Offset yield stress (MPa)	Tensile strength (MPa)
300	0.087	271	775	941
400	0.145	396	1,108	1,252
500	0.251	487	1,411	1,632
550	0.336	581	1,769	2,057

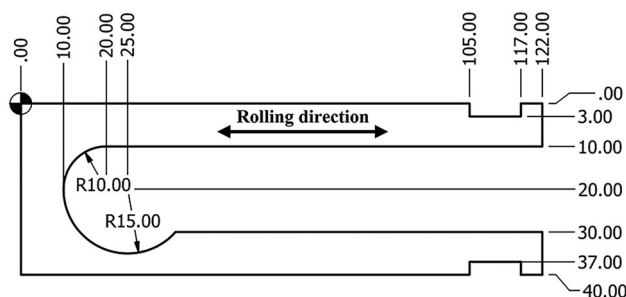


FIGURE 1 The illustration of the tuning-fork specimen with rolling direction marked with an arrow sign. Dimensions are in mm and specimen thickness is 5 mm

Based on the tensile test results of each steel grade, FEM models were built with Abaqus 2019 to calculate the arm distance range for the complete elastic region with the specimen arms pushed towards each other. Due to the geometry of the specimens, the main tensile stress concentration was only at the outer part of the narrower arm, as presented in Figure 2.

Before testing, the outer part of the narrower arm was mechanically polished with a Buehler polishing machine using up to 240 grit discs. Afterwards, the specimens were ultrasonically cleaned and finally stressed with a specially designed clamp (Figure 3). The clamp was designed for an equal stress distribution with a clamping screw, allowing only the compressive inward movement, which was used to create the elastic tensile stress needed. A small rectangular pressing piece was used at the end of the screw to guarantee an even pressure during clamping. The pressing piece was manufactured to fit into the slot in the specimen arm. This was the latest implementation of the test rig with the potentiostatic hydrogen charging. The final fracture occurred always on the narrower side of the specimen.

2.2 | Electrochemical hydrogen charging and the charging cells

Constant displacement tests were performed at room temperature with both galvanostatic and potentiostatic

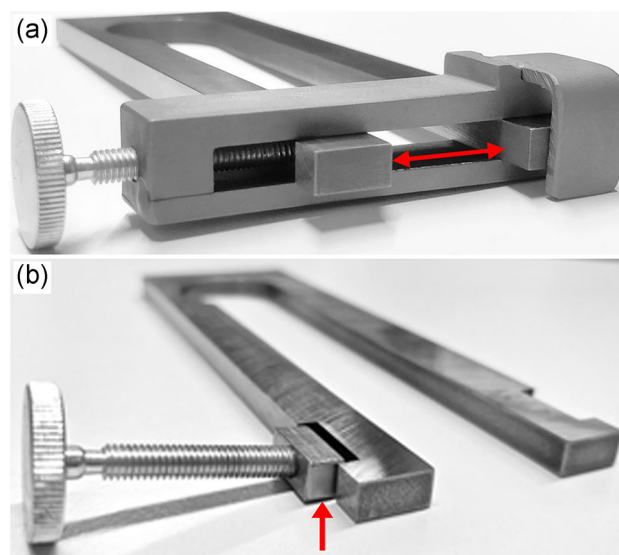


FIGURE 3 (a) The clamping arrangement with a screw adjusting the arm distance and (b) the location of pressing piece for an even pressure distribution [Color figure can be viewed at wileyonlinelibrary.com]

techniques (VersaSTAT3 Potentiostat) using a 0.1-M $\text{H}_2\text{SO}_4 + \text{CH}_4\text{N}_2\text{S}$ (5 g/L) electrolyte. In both set-ups, the counter electrode was a coated titanium mesh, with oxide coating in the galvanostatic set-up and platinum coating in the potentiostatic set-up. The reference electrode used in the potentiostatic hydrogen charging was an $\text{Hg}/\text{Hg}_2\text{SO}_4$ electrode placed in a Luggin capillary. During the galvanostatic hydrogen charging, a constant current density of $10 \text{ mA}/\text{cm}^2$ was applied.

To select an appropriate cathodic potential for hydrogen charging of the test materials, polarisation was performed between $-1,500$ and $1,500 \text{ mV}$. The samples showed a cathodic Tafel behaviour to the corrosion potential of approximately $-1,000 \text{ mV}$; therefore the potential level of $-1,200 \text{ mV}$ was selected for the potentiostatic hydrogen charging. The polarisation curves are given in Figure 4.

The original TFT cell was designed for the galvanostatic hydrogen charging with two electrodes, a working electrode and a counter electrode, with no electrolyte circulation system (Figure 5a). Teflon tape was used to

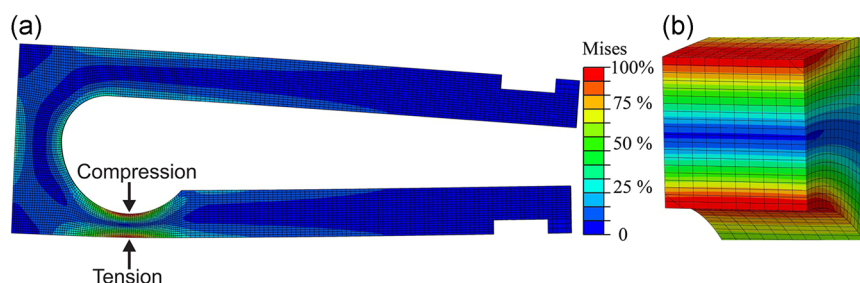


FIGURE 2 (a) The normalised stress state in the tuning-fork test specimen that has been compressed to its yield limit, where red colour represents the high-stress regions and (b) the stress state on the expected crack plane [Color figure can be viewed at wileyonlinelibrary.com]

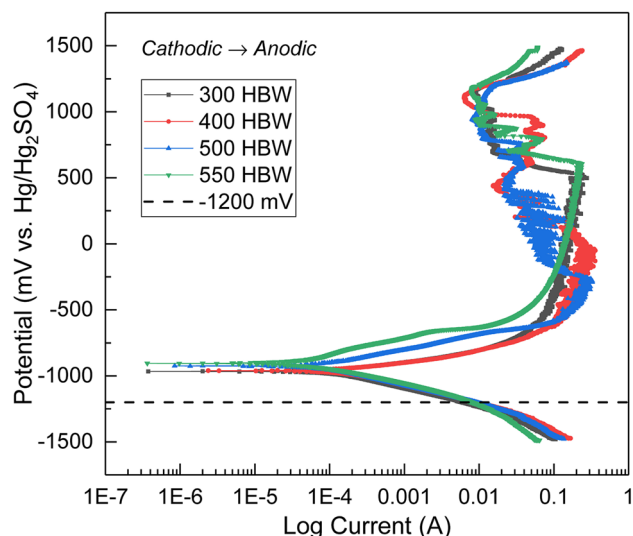


FIGURE 4 Polarisation curves of the tested steel grades in a 0.1-M H_2SO_4 + 5 g/L thiourea solution at a scan rate of 1 mV/s at room temperature [Color figure can be viewed at wileyonlinelibrary.com]

ensure that the active surface area exposed to hydrogen charging remained constant.^[19]

To enable the potentiostatic hydrogen charging, a special electrochemical cell design was introduced to ensure a fixed location of all the electrodes, particularly the reference electrode. The design comprises of a glass beaker with a removable plastic cap with holes for electrodes. A new arrangement was also used to control the electrolyte circulation while maintaining the same electrolyte level. First, the electrolyte was deaerated by nitrogen gas and stirred in a reservoir bottle, which had a bottom hose outlet. The hose was connected to the corrosion cell, where the electrolyte was pumped with a flow

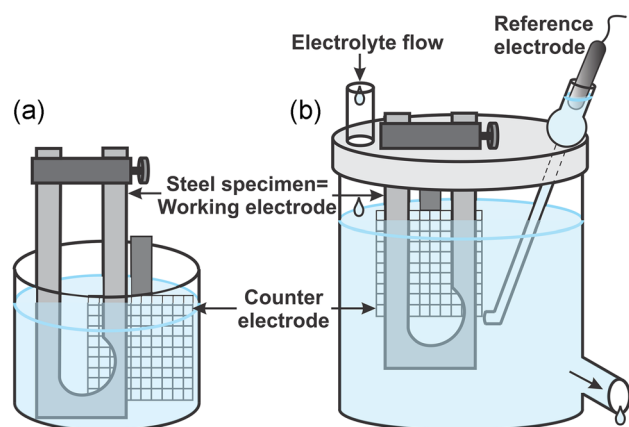


FIGURE 5 A schematic presentation of the corrosion cells utilised in hydrogen charging: (a) galvanostatic corrosion cell and (b) potentiostatic corrosion cell [Color figure can be viewed at wileyonlinelibrary.com]

velocity adjusting stopcock. The corrosion cell contained also a bottom hose outlet with another stopcock, which led to a waste container. Therefore, the circulation of the electrolyte was controlled by adjusting stopcocks, which regulated the incoming and outgoing flow velocity of the electrolyte in the corrosion cell. The corrosion cells for the galvanostatic and potentiostatic set-ups are presented in Figure 5.

2.3 | SCC susceptibility evaluation

In this study, the SCC susceptibility was evaluated by establishing an approximately 25-MPa stress difference between the lowest fracture stress (F) and the highest no-fracture stress (NF) results with 24-hr tests. The no-fracture result was established multiple times for each steel grade, in addition to other tests confirming the lowest fracture stress. When necessary, the binary search procedure for threshold stress from the standard for stress corrosion testing SFS-EN ISO 7539-1 was employed.^[24] To enable the comparison of the different steel grades, the applied stress was presented as a percentage value from the tensile strength of each material. Furthermore, fractography was used to identify the crack initiation sites and the crack propagation mechanism.

3 | RESULTS AND DISCUSSION

3.1 | Galvanostatic versus potentiostatic hydrogen charging

To compare the galvanostatic and potentiostatic hydrogen charging techniques, each fracture and no-fracture results are presented as a percentage value from the tensile strength of the material. Figure 6 comprises all the results obtained from the hydrogen charging tests, showing the dependence of the threshold stress value on the steel hardness, but excluding the overlapping readings at each measuring point for the sake of readability. Both hydrogen charging techniques produced similar results, showing that the fracture stress decreases with the increasing hardness of the steel.

A good resistance to hydrogen was detected with the 300-HBW steel grade. When the constant potential was applied, the 300-HBW steel grade did not fracture under any circumstances within the maximum test time of 24 hr, not even with stress exceeding the yield strength of the material. However, with the galvanostatic hydrogen charging, the 300-HBW steel grade fractured if the applied stress was in the close proximity of the yield strength of the material. Also, with the galvanostatic

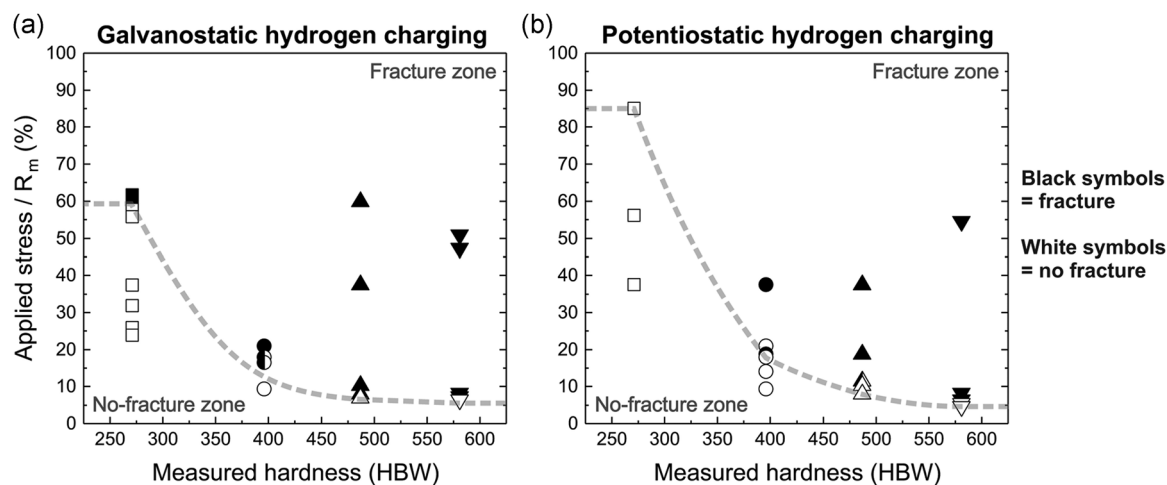


FIGURE 6 The comparison of the fracture and no-fracture stress results for (a) galvanostatic and (b) potentiostatic hydrogen charging

technique, hydrogen blisters were observed on the testing surface of the 300-HBW steel grade specimens with the unaided eye. The appearance of hydrogen blisters can be a consequence of the excessive current density or charging time.^[25,26] If hydrogen absorption on the surface is higher than the diffusion into the substrate, molecular hydrogen can form beneath the metal surface in suitable voids due to the high local concentrations of atomic hydrogen.^[27] The generated substantial pressure then leads to the formation of hydrogen blisters. Normally, hydrogen-induced blistering is prevalent for low-strength alloys and they are considered resistant to HE.^[8]

With both hydrogen charging techniques, the results for the 400-HBW steel grade were not conclusive due to the excessive scatter in the results with varying fracture and no-fracture results. The ambiguous results may be explained by a lower HE susceptibility, as the carbon content and the strength level were significantly lower, compared with those of the 500-HBW steel grade. The reason may also be an inhomogeneous microstructure, but this demands further investigations.

Furthermore, 500- and 550-HBW steel grades, which are more susceptible to hydrogen, manifested good reproducibility of the results with both hydrogen charging set-ups. Figure 7 presents the results of galvanostatic and potentiostatic hydrogen charging, where the higher slope represents the larger differences in the results.

Potentiostatic hydrogen charging showed a better resolution judged by the fact that it produced larger differences between the lowest fracture stress results. The biggest difference between the cell set-ups was the use of reference electrode in the potentiostatic hydrogen charging for the controlled potential on the surface of all the test materials and therefore the same hydrogen activity.^[16–18] During the galvanostatic hydrogen charging, the potential was not

controlled or measured on the specimen surface. Furthermore, the galvanostatic set-up also lacked the electrolyte circulation and level control, which could have affected the amount of hydrogen produced during the 24-hr charging procedure. The magnitude of the applied current density can certainly affect the results too based on the evidence of hydrogen-induced blistering.

For both techniques, the observed stress levels below which the cracking did not occur were very low. The reported values of this environmental-threshold stress level have been approximately 10% from the yield strength of the material, and therefore hydrogen charging conditions may have been too severe, and require corrective adjustments towards a milder test environment.^[7] This type of environment could be achieved, for example, by lowering the applied current density/potential, or by reducing the amount of thiourea ($\text{CH}_4\text{N}_2\text{S}$), which acts as

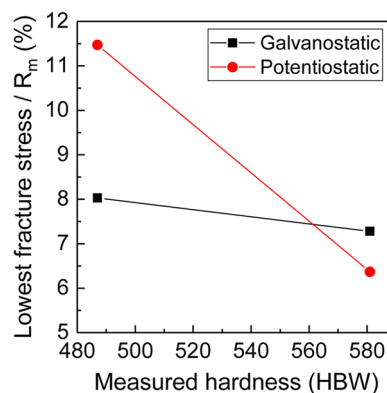


FIGURE 7 The comparison of the lowest fracture stress results of 500- and 550-HBW steel grades tested with galvanostatic and potentiostatic set-ups [Color figure can be viewed at wileyonlinelibrary.com]

a poison against hydrogen recombination and increases hydrogen absorption.

3.2 | Fractography

After hydrogen charging tests, pitting corrosion was identified on all the specimen surfaces that were immersed into the electrolyte. Pitting corrosion most likely results from near-surface nonmetallic inclusions, which can contribute to the crack initiation process. The 300-HBW test specimens experienced also hydrogen-induced blistering. Figure 8 demonstrates the differences between typical specimen surfaces with pitting corrosion and a hydrogen blister. The fractured specimens were cut, and fracture surfaces were treated chemically by immersion in a specific solution (50-ml HCl, 450-ml distilled water and 15-g hexamethylenetetramine) to remove the corrosion products. Selected fracture surfaces from the lowest fracture stress tests were investigated with a Zeiss Sigma field emission scanning electron microscope (SEM) to identify the crack initiation site and crack propagation mechanism. The overall view of the whole fracture surface area was obtained with a TESCAN VEGA3 SEM.

In all cases, the crack initiation started at one of the corners/edges of the tensile stress areas, as demonstrated in Figure 9. The crack propagation mechanism in the 500- and 550-HBW steel grades with reproducible results was also investigated. All the fracture surfaces manifested the similar quasi-cleavage fracture morphology,^[28] as shown in Figure 10, but the 550-HBW steel grade exhibited more secondary cracking, which is marked with white arrows (Figure 10).

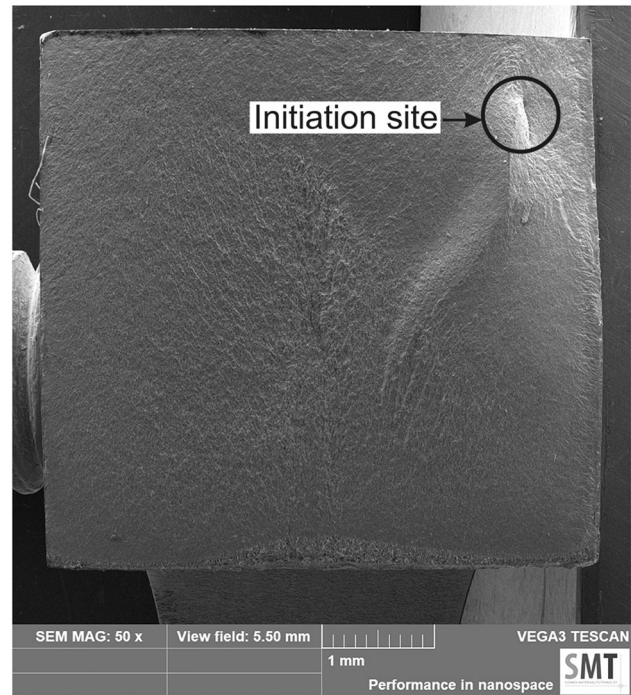


FIGURE 9 The fracture surface of a 500-HBW steel specimen exhibiting the initiation site of the final fracture and a completely flat fracture mode

4 | CONCLUSIONS

This study presents the development work of the novel TFT and expands the previously presented test data of Latypova et al.^[19] Direct-quenched steel grades with nominal hardness levels of 300, 400, 500 and 550 HBW were tested in the galvanostatic and potentiostatic corrosion cells with special tuning-fork specimens to

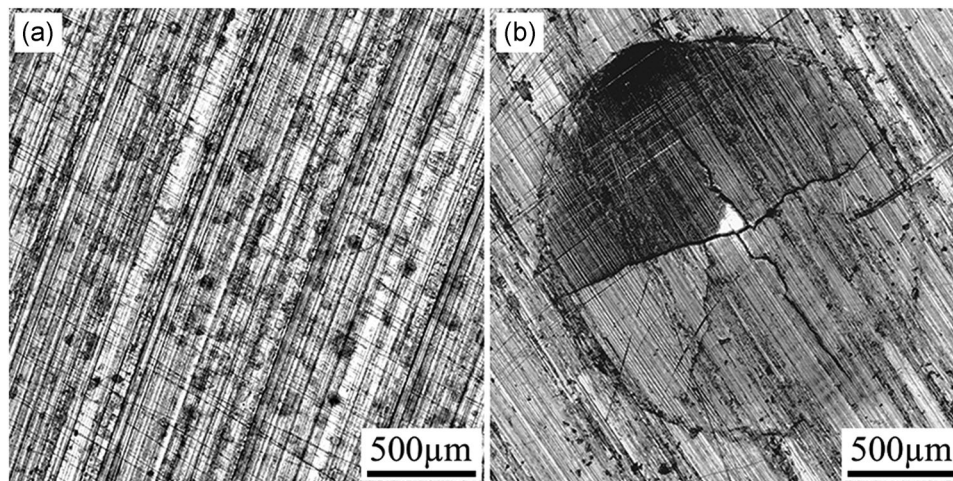


FIGURE 8 (a) The typical surface with pitting corrosion on a 500-HBW steel specimen and (b) a hydrogen blister visible after hydrogen charging on a 300-HBW steel specimen. Laser scanning confocal microscope images

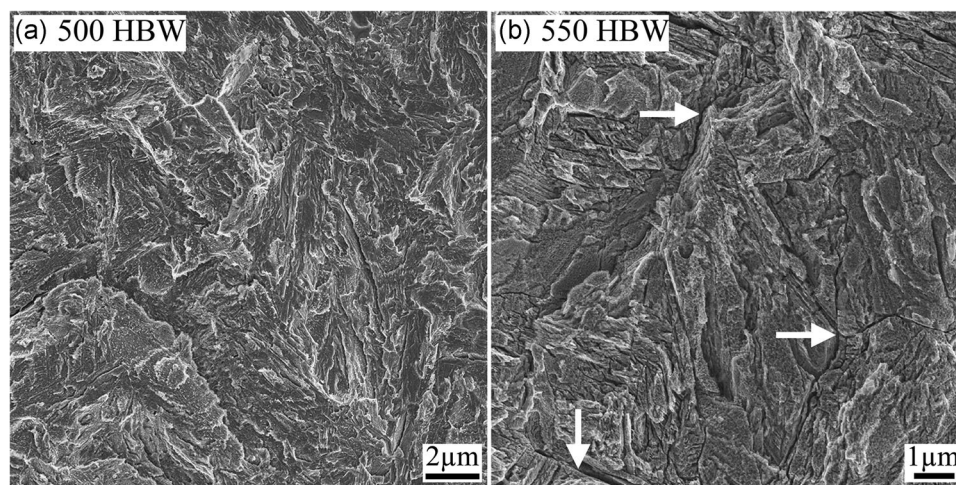


FIGURE 10 Hydrogen-induced quasi-cleavage fracture surfaces of (a) 500-HBW and (b) 550-HBW steel grades, with white arrows highlighting secondary cracks

evaluate their susceptibility to HISCC. Specimens were elastically stressed via a constant displacement and exposed to cathodic hydrogen charging conditions to determine the lowest F and highest NF stress. The original cell was utilised for the galvanostatic hydrogen charging, and the newly developed cell was adapted for the potentiostatic technique. Each steel grade was tested in both cells to investigate the effects of the different hydrogen charging techniques on the lowest fracture stress level.

Both galvanostatic and potentiostatic hydrogen charging produced similar results, where the lowest fracture stress decreased with the increased hardness. Severe hydrogen charging conditions had only a minor effect on the 300-HBW steel grade. The 400-HBW steel grade showed excessive scatter with the overlapping NF and F values that it was not possible to determine the reliable threshold stress level for it. However, the 500- and 550-HBW steel grades demonstrated reliable results with good reproducibility, which indicates that the lower hardness steel grades were not susceptible enough to HE in the used test conditions.

Comparing the charging techniques, the potentiostatic hydrogen charging produced results with a better resolution due to the larger differences between the different steel grades. The results can be explained by the superior potential control and the same hydrogen activity on all the studied steels during the potentiostatic hydrogen charging. Therefore, in the case of steels with very high hardness, the potentiostatic hydrogen charging method is considered to be more reliable when compared with the galvanostatic hydrogen charging in these specific test conditions. The lowest fracture results for the 500- and 550-HBW steel grades were, however, very low;

therefore, a milder test environment could potentially lead to an even better resolution.

ACKNOWLEDGEMENTS

The authors wish to thank the technical staff from the Materials and Mechanical Engineering unit at the University of Oulu for their help with the experiments and sample preparation. Sakari Pallaspuuro acknowledges Academy of Finland (#311934) for funding. This study was supported by Business Finland Oy. The FEM models created by Oskari Seppälä and SEM operation by Oskari Ryti are greatly acknowledged.

ORCID

Renata Latypova  <http://orcid.org/0000-0002-5052-8191>

REFERENCES

- [1] J. Kömi, P. Karjalainen, D. Porter, *Encyclopedia of Iron, Steel, and Their Alloys*, CRC Press, Boca Raton, FL **2016**.
- [2] S. Pallaspuuro, *Ph.D Thesis*, University of Oulu, Finland, **2018**.
- [3] R. A. Cottis, *Stress Corrosion Cracking—Guides to Good Practice in Corrosion Control*, National Physical Laboratory, Teddington, UK **2000**.
- [4] R. H. Jones, *Stress-Corrosion Cracking*, ASM International, Materials Park, OH **1992**.
- [5] S. Ramamurthy, A. Atrens, *Corros. Rev.* **2013**, 31, 1.
- [6] J. Woodtli, R. Kieselbach, *Eng. Fail. Anal.* **2000**, 7, 427.
- [7] W. C. Lyons, G. J. Plisga, M. D. Lorenz, *Standard Handbook of Petroleum and Natural Gas Engineering*, Gulf Professional Publishing, Houston, TX **2016**.
- [8] *ASM Handbook Volume 11: Failure Analysis and Prevention* (Eds: W. T. Becker, R. J. Shipley), ASM International, Materials Park, OH **2002**.
- [9] N. Eliaz, A. Shachar, B. Tal, D. Eliezer, *Eng. Fail. Anal.* **2002**, 9, 167.

- [10] *ASM Handbook Volume 13C: Corrosion: Environments and Industries* (Eds: S. D. Cramer, B. S. Covino), ASM International, Materials Park, OH **2006**.
- [11] R. Heidersbach, *Metallurgy and Corrosion Control in Oil and Gas Production*, John Wiley & Sons, Hoboken, NJ **2011**.
- [12] L. Bertolini, B. Elsener, P. Pedferri, R. Polder, *Corrosion of Steel in Concrete Corrosion*, John Wiley & Sons, Hoboken, NJ **2004**.
- [13] P. C. Fernández, *Development of an Optimized Methodology for Tensile Testing of Carbon Steels in Hydrogen Environment*, Research Centre for the Application of Steels, Zelzate, Belgium **2009**.
- [14] E. Akiyama, S. Li, *ECS Trans.* **2017**, 75, 23.
- [15] Metrohm, *Autolab Application Note EC08*, **2011**.
- [16] O. Todoshchenko, *Ph.D Thesis*, Aalto University, Finland, **2015**.
- [17] T. Hickel, R. Nazarov, E. McEniry, Z. Zermout, Y. Yagodzinsky, H. Hänninen, O. Rott, R. Thiessen, K. Mraczek, *Hydrogen Sensitivity of Different Advanced High Strength Microstructures (HYDRAMICROS)*, Publications Office of European Union, Luxembourg, UK **2013**.
- [18] Y. Yagodzinsky, O. Todoshchenko, S. Papula, H. Hänninen, *Steel Res. Int.* **2011**, 82, 20.
- [19] R. Latypova, T. Kauppi, S. Mehtonen, H. Hänninen, D. Porter, J. Kömi, *Mater. Corros.* **2018**, 70, 521.
- [20] ASTM G38-01, Standard practice for making and using C-ring stress-corrosion test specimens, **2001**.
- [21] *SFS-EN ISO 7539-5*, Corrosion of metals and alloys. Stress corrosion testing. Part 5: Preparation and use of C-ring specimens, **1989**.
- [22] *ASTM G30-97*, Standard practice for making and using U-bend stress-corrosion test specimens, **2016**.
- [23] *SFS-EN ISO 7539-3*, Corrosion of metals and alloys. Stress corrosion testing. Part 3: Preparation and use of U-bend specimens, **1995**.
- [24] *SFS-EN ISO 7539-1*, Corrosion of metals and alloys. Stress corrosion testing. Part 1: General guidance on testing procedures, **2012**.
- [25] D. Pérez Escobar, C. Miñambres, L. Duprez, K. Verbeken, M. Verhaege, *Corros. Sci.* **2011**, 53, 3166.
- [26] G. Mertens, L. Duprez, B. C. De Cooman, M. Verhaege, *Adv. Mater. Res.* **2007**, 15–17, 816.
- [27] J. Rehrl, K. Mraczek, A. Pichler, E. Werner, *Mater. Sci. Eng., A* **2014**, 590, 360.
- [28] M. L. Martin, J. A. Fenske, G. S. Liu, P. Sofronis, I. M. Robertson, *Acta Mater.* **2011**, 59, 1601.

How to cite this article: Latypova R, Nyo TT, Kauppi T, et al. Hydrogen-induced stress corrosion cracking studied by the novel tuning-fork test method. *Materials and Corrosion*. 2020;1–8.
<https://doi.org/10.1002/maco.202011767>